Received: 10 June 2024 | Revised: 19 September 2024 | Accepted: 15 October 2024

DOI: 10.1111/cas.16382

Cancer Science WILEY

ORIGINAL ARTICLE

Zymogen granule protein 16B (ZG16B) is a druggable epigenetic target to modulate the mammary extracellular matrix

Máté Lengyel[1,2] | Ádám Molnár[1] | Tamás Nagy[3] | Sham Jdeed[1,2] | Ildikó Garai[3] | Zsolt Horváth[4] | Iván P. Uray[1,2,5]

[1]Department of Clinical Oncology, Faculty of Medicine, University of Debrecen, Debrecen, Hungary

[2]The Molecular Cell and Immune Biology Doctoral School, University of Debrecen, Debrecen, Hungary

[3]Department of Nuclear Medicine, University of Debrecen, Debrecen, Hungary

[4]Center of Oncoradiology, Bács-Kiskun County Teaching Hospital, Kecskemét, Hungary

[5]Department of Biochemistry and Molecular Biology, University of Debrecen, Debrecen, Hungary

Correspondence
Iván P. Uray, Department of Clinical Oncology, Faculty of Medicine, University of Debrecen, Nagyerdei krt. 98, Debrecen 4032, Hungary.
Email: uray.ivan@med.unideb.hu

Funding information
National Excellence program of the Ministry for Innovation and Technology, Hungary, Grant/Award Number: ÚNKP-21-3; National Research, Development and Innovation Office of Hungary, Grant/Award Number: K129218; European Social Fund, Grant/Award Number: GINOP 2.3.2-15 2016-00020; University of Debrecen Scientific Research Bridging Funds (DETKA and ÁOK), Grant/Award Number: DE 37-11/2024

Abstract

High tissue density of the mammary gland is considered a pro-tumorigenic factor, hence suppressing the stimuli that induce matrix buildup carries the potential for cancer interception. We found that in non-malignant mammary epithelial cells the combination of the chemopreventive agents bexarotene (Bex) and carvedilol (Carv) suppresses the zymogen granule protein 16B (ZG16B, PAUF) through an interaction of ARID1A with a proximal enhancer. Bex + Carv also reduced ZG16B levels in vivo in normal breast tissue and MDA-MB231 tumor xenografts. The relevance of ZG16B is underscored by ongoing clinical trials targeting ZG16B in pancreatic cancers, but its role in breast cancer development is unclear. In immortalized mammary epithelial cells, secreted recombinant ZG16B stimulated mitogenic kinase phosphorylation, detachment and mesenchymal characteristics, and promoted proliferation, motility and clonogenic growth. Highly concerted induction of specific laminin, collagen and integrin isoforms indicated a shift in matrix properties toward increased density and cell-matrix interactions. Exogenous ZG16B alone blocked Bex + Carv-mediated control of cell growth and migration, and antagonized Bex + Carv-induced gene programs regulating cell adhesion and migration. In breast cancer cells ZG16B induced colony formation and anchorage-independent growth, and stimulated migration in a PI3K/Akt-dependent manner. In contrast, Bex + Carv inhibited colony formation, reduced Ki67 levels, ZG16B expression and glucose uptake in MDA-MB231 xenografts. These data establish ZG16B as a druggable pro-tumorigenic target in breast cell transformation and suggest a key role of the matrisome network in rexinoid-dependent antitumor activity.

KEYWORDS
ARID1A, ECM, rexinoid, ZG16B

1 | INTRODUCTION

While over 15% of breast cancer cases develop without an addiction to either estrogen receptors or Her2 receptors, RXR-selective retinoids have a well documented ability to suppress receptor-negative breast cancer formation in transgenic mouse models.[1–3] We hypothesized that the rexinoid-dependent suppression of pro-tumorigenic factors in premalignant breast cells represents valid targets for cancer interception and the inhibition of cellular transformation. Previously we demonstrated that the clinically available rexinoid bexarotene (Bex) augmented by carvedilol (Carv) suppressed TGFβ signaling in normal breast epithelial cells, implying that the extracellular matrix (ECM) may be a relevant tumor suppressive target for chemopreventive agents.[4] However, a central mediator of cell-matrix interactions in breast cells has not been identified.

ZG16B (pancreatic adenocarcinoma upregulated factor, PAUF) is a mammalian lectin secreted by acinar cells, and known to exert tumor-promoting activity in cancer cells through autocrine and paracrine mechanisms.[5,6] The relevance of ZG16B in the progression of pancreatic and ovarian cancers is indicated by ongoing clinical trials (NCT05141149) evaluating the effectiveness of agents targeting ZG16B. Reduction of circulating ZG16B levels may improve clinical outcomes through the modulation of the tumor matrisome.[7,8] Although ZG16B was also proposed as a prognostic marker in breast cancer, the impact of ZG16B expression in breast carcinogenesis has not been examined.[9]

Clinically, increased mammographic density of the breast has been recognized as a major risk factor for tumorigenesis.[10] Moreover, a role for mammary tissue remodeling based on altered matrix composition in the course of malignant transformation has also been documented.[11,12] Elevated ECM density and alignment are associated with increased ECM stiffness and tumor progression.[13,14] We demonstrate that ZG16B stimulates the expression of a cadre of proteins critical for ECM formation, and cell-matrix interactions and antagonizes Bex+Carv in limiting proliferation and motility. Identified as an epigenetic mechanism, the regulation of ZG16B controlling ECM remodeling emerges as a key target of rexinoid-based chemopreventive activity.

2 | MATERIALS AND METHODS

2.1 | Cell lines and cell culture

The HEK293 (CVCL_0045) cell line was purchased from the ATCC and used at low passage numbers. MCF7, T47D, MDA-MB-231, MDA-MB-468, HCC1143 cell lines and human mammary epithelial cells immortalized by telomerase, HME-hTert, were a kind gift from Dr. Powel H. Brown (MD Anderson Cancer Center). MCF7, T47D, and HEK293 cells were grown in DMEM; MDA-MB-231, MDA-MB-468, HCC1143, and HEK293 cells were grown in RPMI-1640 medium with 10% fetal bovine serum and 1% penicillin–streptomycin–L-glutamine. HME-hTert cells were grown in Mammary Epithelial Basal Medium (MEBM) basal medium supplemented with Mammary Epithelial Cell Growth Media (MEGM) growth factor SingleQuots (Lonza, Basel, CH). Authentication of cell lines was performed by deep sequencing before the study. All cell lines were regularly tested for *Mycoplasma*-free conditions using the Promokine PCR-based assay.

2.2 | ChIP-Seq and quantitative PCR analysis

Chromatin immunoprecipitation (ChIP) from HME-hTert cells was conducted as reported.[4] Differential recruitment of ARID1A and H3K27ac to genomic regions upon Bex+Carv was detected by massively parallel sequencing (ChIP-seq) and analyzed using the Galaxy (https://usegalaxy.eu/) platforms.[4] Peaks were called using MACS2 software.

ChIP-seq results were confirmed by SYBR green-based quantitative PCR of ChIP samples. The amounts of DNA fragments associated with ARID1A or H3K27ac were normalized to input samples.

To quantitate mRNA transcript levels by RT-qPCR, gene-specific FAM-BHQ dual-labeled TaqMan probes and primers were designed. mRNA copy numbers were determined relative to a standard dilution series of single-stranded DNA amplicons. Target gene expression was normalized to β-actin and shown as relative values.

2.3 | In silico prediction of transcription factor binding sites on ZG16B gene promoter and enhancer region

Genomic sequences were obtained from the NCBI Nucleotide database. Promoter region: *Homo sapiens* chromosome 16, GRCh38.p14, NC_000016.10:2828303-2830303; Enhancer region: *Homo sapiens* chromosome 16, GRCh38.p14, NC_000016.10:28855872886195. For the in silico prediction of transcription factor binding sites (TFBS), Promo tool by ALGGEN (Version: 3.0.2) was used, filtering for human transcription factors and binding sites (Figure S1). The maximal dissimilarity rate was set to 5%.

2.4 | Immunofluorescence and histochemical labeling of ZG16B and mesenchymal markers

This procedure was conducted as reported previously.[13] A list of antibodies used is shown in Table S1.

2.5 | Immunohistochemical detection of ZG16B in non-transformed breast tissues

Ten 4-month-old FVB-MMTV-ErbB2 mice were treated with vehicle or Bex+Carv (20 mg/kg each) by oral gavage five times per week.

Mice were euthanized and mammary glands harvested at 6 months of age. Experimental animals were kept under standard housing conditions at MD Anderson Cancer Center (MDACC) animal facilities; all animal procedures were reviewed and approved by MDACC. Tissues were mounted onto slides and processed for immunohistochemistry as previously described.[15] Four samples per group showing no signs of early lesions were labeled with ZG16B antibody and DAPI. ZG16B positivity was determined using a watershed function and positive areas were compared between groups.

2.6 | Analysis of The Cancer Genome Atlas (TCGA) datasets

To compare ZG16B expression of multiple cancer types the TCGA Pan-Cancer dataset was selected with a total number of 12,839 samples, and analyzed in UCSC Xena browser (https://xena.ucsc.edu/). Genomic subtype, ZG16B expression and primary disease were used as variables. To compare ZG16B expression between healthy mammary tissue and breast cancer data from the TCGA Research Network (http://cancergenome.nih.gov/) were analyzed.

2.7 | Construction of ZG16B-EGFP expression vector and generation of ZG16B-containing conditioned supernatant

ZG16B mRNA was transcribed to cDNA from HME-hTert total RNA samples by reverse transcription. The amplified gene-specific DNA fragment was gel purified, directionally cloned into the pEGFP-C3 plasmid using the *Eco*RI and *Sal*I restriction sites, and sequence verified.

To produce soluble ZG16B, HEK293 cells in serum-free medium were transfected with empty pEGFP-C3 or pEGFP-ZG16B vectors. Supernatants and cell lysates were collected after 48 h of transfection. Supernatants were passed through 30 and 10 kDa size-exclusion columns. Cellular ZG16B expression was confirmed by western blotting, fluorescence microscopy and tandem mass spectrometry (Figures S2 and S3). Secreted ZG16B in conditioned, concentrated supernatants was identified as an ~16 kDa size band in western blotting (Figure 2A), confirming that EGFP was cleaved from ZG16B upon secretion.

2.8 | Microscopy-based 2D proliferation assay

Breast cells were treated on 96-well optical plates at low density and fixed using 4% formaldehyde after 4 days. Sample processing, microscopy and data collection were performed as reported.[4] The counting algorithm containing contrast enhancement and thresholding of 8-bit images in a looped macro identified objects were separated by the watershed function and lower/upper size limits were applied ($5 < x < 400$ in pixels) to exclude clumped cells and debris.

2.9 | In vitro cell migration (scratch) assay

HME-hTert cells were plated on Ibidi culture inserts. After 24 h, inserts were removed and cells treated. Before (T-Start) and after treatment (T-End) the scratch area was imaged using a DMi8 inverted fluorescence microscope (Leica Microsystems, Wetzlar, Germany) with a ×10 objective. Images were individually evaluated by creating masks after contrast enhancement, minimal object size filtering and thresholding. Scratch edges were labeled manually and the cell-free space was measured and compared at the T-Start and T-End time points. For drug modulation, cells were pre-treated with Veh or Bex + Carv 48 h before plating for scratch assay. ZG16B treatment was applied for 24 h after scratching the cell monolayer.

2.10 | Cell adhesion assay

Cells were seeded onto 24-well plates and pre-treated for 48 h with control supernatant or conditioned medium containing ZG16B, labeled with Hoechst stain and washed with PBS. Stained cells were incubated with 0.25 mg/mL trypsin–EDTA for 5 min. Following trypsinization, detached cells were fremoved in a PBS wash, and attached cells were imaged and counted by microscopy. Trypsinizing and imaging steps were repeated for a total of 25 min.

2.11 | Analysis of cellular morphology

Normal cells were plated onto 96-well optical plates and treated with concentrated supernatant from ZG16B-transfected HEK293 cells or TGFβ (10 μM), with or without ZG16B neutralizing antibody (16 ng/μL). Treatments were repeated every 48 h. After 5 days, cells were fixed in 4% formaldehyde and stained with DAPI, HCS-CellMask-Red and Phalloidin-A488. Microscopic images were analyzed with CellProfiler, measuring circularity and axis ratios on a cell-by-cell basis.

2.12 | Gene expression analysis using RNA-Seq

Transcriptomic profiling of HME-hTert cells was conducted relative to vehicle effects, following a 6-h exposure to ZG16B, or 24 h of Bex + Carv, respectively. Sequencing was performed on the Illumina platform. Fastq.gz files were uploaded to Galaxy, and trimmed by the Trimmomatic tool using the slidingwindow and minlen operations. HISAT2 was used for alignment using the human (*Homo sapiens*) (b37): hg19 genome gene expression was quantified using the Featurecounts tool. Differentially expressed genes were identified with DeSeq2 and filtered by the $p < 0.01$ value. Differentially expressed genes from ZG16B and Bex + Carv treatments were merged, and genes modulated by both treatments were identified, clustered by Cluster 3.0 and TreeView. Gene ontology and network analyses of inversely regulated

genes were performed using String (Version: 11.5). Gene expression datasets are public under accession numbers PRJNA965935, PRJNA965937, PRJNA966894.

2.13 | Measurement of kinase activation by western blotting

Cell lysates were prepared using RIPA buffer and the phosphorylated and total protein amounts were measured as reported.[4] Target proteins were detected on 10% PAGE using primary antibodies in 5% BSA-TBST. Kinase activation was assessed by phosphorylated relative to total kinase levels. All antibodies used are listed in Table S1. LY294002 was a kind gift from Dr. Zoltán Balajthy.

2.14 | Non-adherent tumorsphere formation assay

To examine anchorage-independent growth, 10^4 MCF7, T47D and MDA-MB-231 breast cancer cells were incorporated in 0.3% top layer agarose gel supplemented with DMEM. Tumor cells were pre-treated for 48 h with DMSO, Bex (1 μM), Carv (1 μM), Bex + Carv (1 μM each), control, or ZG16B-enriched supernatants. After 3 weeks of colony growth, phase contrast images were taken in the 3D stack by widefield microscopy and projected to 2D images to count colonies.

2.15 | In vivo xenograft model in SCID mice

Eight female CB17 (IcrHan Hsd-Prkdc) severe combined immunodeficiency (SCID) mice (Akronom Ltd., Budapest, Hungary) were grafted with 5 million MDA-MB-231 cells mixed with an equal volume of Matrigel, next to the lower mammary glands. The administration of vehicle or Bex + Carv started in randomized groups of four mice when the tumors reached 100 mm^3, and continued to 1000 mm^3 in size. Experimental agents and vehicles were homogenously distributed in ground chow and re-formed into pellets, with consumption recorded. Tumor sizes were monitored using calipers twice a week. At the start and conclusion of the treatments, 20-min whole-body PET-NMR spectroscopy (nanoScan PET/NMR 1T, Mediso Ltd., Hungary) was performed to determine glucose uptake of intravenously injected 15 MBq ^{18}F-fluoro-2-deoxy-D-glucose (^{18}FDG). Collected tumors were weighed, halved, and fixed in paraformaldehyde for IHC, RNA and protein extraction. Experimental animals were kept and treated in accordance with all requirements of the Hungarian Ethical Laws and regulations of the European Union (permit number: 16/2020/DEMÁB).

2.16 | Immunohistochemistry of paraffin-embedded tissues

Sections were cut into slices of 5-μm thickness, deparaffinized using xylene substitute and rehydrated using an ethanol series. Antigens were retrieved in a pressure cooker using citrate buffer (pH 6.0). Blocking and indirect detection were performed using a Vectastain R.T.U. kit and 3,3'-Diaminobenzidine (DAB) substrate, with hematoxylin counterstaining. Following dehydration, sections were mounted using colorless nail polish and imaged under a DMi8 microscope. Image analysis was performed using ImageJ software.

2.17 | Glucose uptake assay

To quantify glucose uptake in vitro, the Cell Meter™ 2-NBDG Glucose Uptake Assay Kit was used. MDA-MB-231 cells in low glucose were treated with DMSO or Bex + Carv (1 μM each) for 1 h before the addition of 2NBDG glucose. Single-cell image analysis was performed using CellProfiler.

2.18 | Statistical analysis

Statistical values are expressed as the average ± SEM. Each experiment contained a minimum of three independent biological replicates. The unpaired Student's *t*-test was performed to compare two groups, and ANOVA was followed by the Mann–Whitney post hoc test for multiple comparisons. A $^*p < 0.05$ represents a significant difference between groups.

3 | RESULTS

3.1 | Epigenetic silencing of ZG16B by cancer suppressive agents in normal mammary epithelial cells

The chemopreventive potential of the rexinoid bexarotene has been shown in animal models, yet its clinical translation is hampered by concerns over untoward side effects.[16] Previously we demonstrated that the adrenergic inhibitor carvedilol augments the suppression of mesenchymal transition and proliferation by low-dose Bex through the redistribution of ARID1A and the SWI/SNF chromatin remodeling complex.[4,17] To identify pro-tumorigenic functions affected by Bex + Carv in telomerase-immortalized human mammary epithelial cells (HME-hTert), we cross-referenced genome-wide changes detected in H3K27 histone acetylation marks with sites of ARID1A enrichment, and suppressed genes in response to the combined Bex + Carv treatment (Figure 1A). The increased occupancy by ARID1A and reduced H3K27 acetylation at the proximal regulatory region of the ZG16B gene were confirmed by qPCR (Figure 1B,C). The detected changes were commensurate with significant downregulation of the mRNA and protein levels of ZG16B. In silico prediction of TFBS at the regulatory regions of ZG16B revealed distinct binding sites for glucocorticoid, estrogen and retinoid X receptors (Figure S1). However, siRNA knockdown of ARID1A completely blocked the ability of Bex + Carv to suppress ZG16B transcription, suggesting a requirement of ARID1A for the combination effect (Figure 1D).

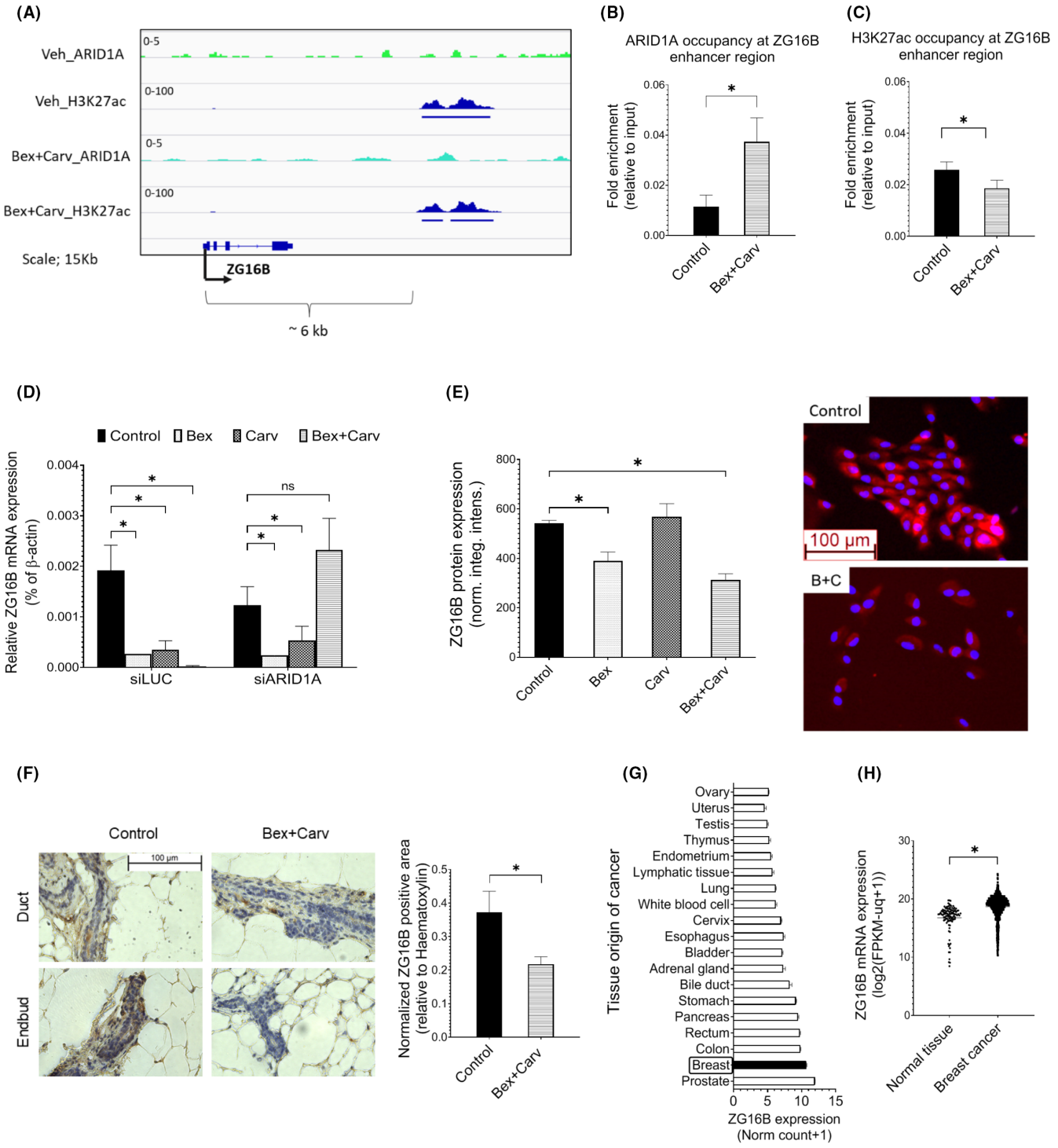

FIGURE 1 Identification of ZG16B as a clinically relevant chemoprevention target. (A) Genome browser view of the ZG16B enhancer region marking ARID1A and H3K27ac recruitment by ChIP-seq analysis following 6-h treatments of HME-hTert cells by vehicle or Bex+Carv (Bex: 100 nM, Carv: 1 μM). (B) Comparison of ARID1A recruitment and (C) H3K27 acetylation at the ZG16B enhancer detected by ChIP-qPCR. (D) ZG16B transcript levels 48 h after transfection with luciferase (LUC) or ARID1A siRNA and 24 h of drug treatment. (E) Comparison of ZG16B protein expression in HME-hTert cells after control, Bex, Carv, Bex+Carv treatments. (F) Comparison of ZG16B protein expression in lesion-free mammary glands of MMVT-ErbB2 transgenic mice after 8 weeks of vehicle or Bex+Carv treatments. (G) Cross-cancer comparison of ZG16B transcript levels in TCGA datasets. (H) Comparison of ZG16B transcript levels in normal versus breast cancer tissues (TCGA). Data represent the mean ± SD (*$p < 0.05$).

Assessed by immune staining, Bex alone or in combination with Carv markedly suppressed ZG16B levels ($p < 0.01$, Figure 1E). Furthermore, in tumor-free, 6-month-old MMTV-ErbB2 mice, long-term Bex+Carv treatment was associated with a marked reduction of ZG16B positivity in microscopically healthy mammary ducts and endbuds (Figure 1F).

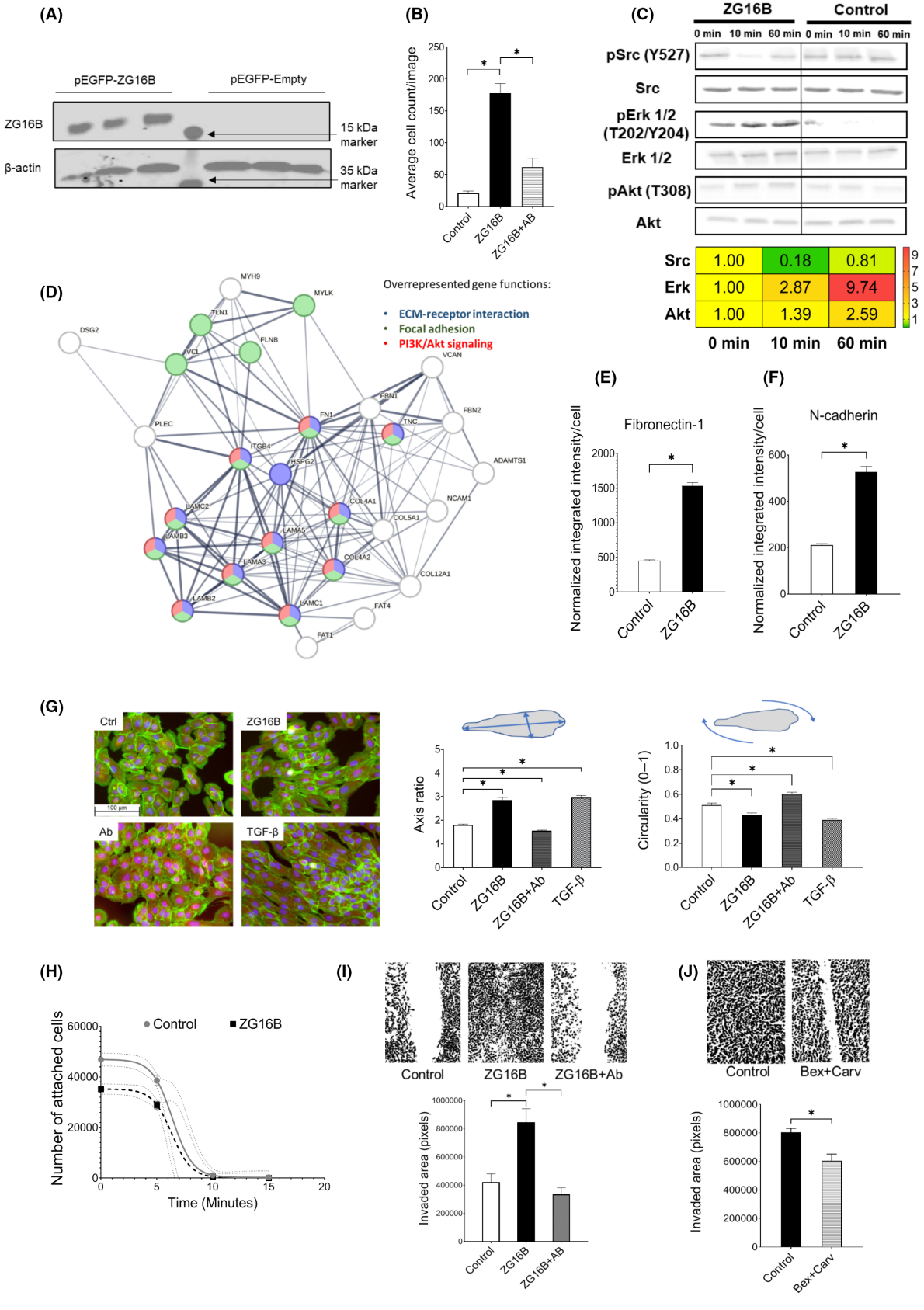

FIGURE 2 ZG16B promotes the growth, migration and mesenchymal characteristics of HME-hTert cells, and concerted changes in cell-ECM interactions. (A) Detection of the ZG16B protein by western blot in supernatants of HEK293 transfected with pEGFP-ZG16B or pEGFP-empty vectors. (B) HME-hTert cell proliferation following a 3-day stimulation with conditioned supernatants. (C) Western blots of Src dephosphorylation (Tyr527 inhibitory site), Erk1/2 and Akt phosphorylation (T202, T308 activating sites) upon ZG16B treatment. Fold changes in phosphorylation normalized to total amounts of kinases are shown in heatmaps. (D) Pathway and gene network analysis of genes induced following 6 h of treatment with ZG16B-enriched supernatant. (E) Comparison of Fibronectin-1 and (F) N-cadherin mesenchymal marker expression upon ZG16B treatment. (G) Single-cell analysis of cell morphology following 5 days of ZG16B or TGFβ (10 μM) treatment. Nuclei were labeled with DAPI (blue), cytoskeleton with Phalloidin-A488 (green) and cell boundaries with CellMask (red). (H) Trypsin-based adhesion assay after 48 h of ZG16B pre-treatment. Cells retained in culture over time during incubation in trypsin solution were counted. (I) Comparison of cell migration upon treatment with conditioned supernatants for 24 h. (J) Comparison of cell migration following pre-treatment with vehicle or Bex + Carv (1 μM each) for 48 h.

ZG16B had first been described as a soluble factor that drives the progression and invasiveness of pancreatic cancer.[6,18] According to TCGA data, breast cancers express ZG16B at the highest levels (Figure 1G). Furthermore, RNA sequencing data indicated that breast cancers express ZG16B at significantly higher levels than normal breast tissue (TCGA, $p < 0.01$; Figure 1H).

3.2 | Recombinant ZG16B regulates growth and the matrisome in non-malignant breast cells

To elucidate its effect on breast cells, the cDNA of ZG16B was cloned into an expression vector behind the EGFP marker gene, expressing a fusion protein upon transient transfection into non-expressing HEK293 cells. Fluorescent staining of uncleaved intracellular ZG16B co-localized with EGFP and the endoplasmic reticulum (Figure S2). However, a natural cleavage site within ZG16B ensured the release of the native protein for secretion, thus processed ZG16B was detected in the cell supernatant (Figure S3). ZG16B peptide fragments were verified in cell extracts by four unique spectra from mass spectrometry after transfection.

HME-hTert cells exposed to ZG16B-containing supernatant markedly increased proliferation, which was mitigated by a ZG16B-specific antibody (Figure 2B). Furthermore, cell populations shifted toward the S and G2/M cell cycle phases upon ZG16B stimulation (Figure S4). Enhanced mitogenic signaling was confirmed by a rapid transitory dip in inhibitory phosphorylation of Src at Tyr527, strong activation of the Erk1/2 kinase (Y204), and a lesser increase in Akt (T308) phosphorylation (Figure 2C) .

The transcriptomic profile of ZG16B-treated HME-hTert cells revealed the overrepresentation of matrix-related genes, consisting of over 50% showing greater than 10% inductions (FDR < 0.1%) (Table 1). While modest in relative values after 6 h of ZG16B exposure, the early-response differences among functional categories affecting stromal density and mechanotransduction appeared highly coordinated. Gene ontology indicated a concerted regulation of gene clusters associated with ECM organization, focal adhesion and PI3K/Akt signaling, potentially representing a pro-tumorigenic profile (Figure 2D). Moreover, ZG16B strongly induced mesenchymal markers, such as fibronectin-1 and N-cadherin, in 24 h (Figure 2E,F). The reprogramming of matrisomal gene expression was associated with clear phenotypic alterations, significant elongation and reduced circularity of the cells (Figure 2G). These changes were also reversed by the co-administration of a neutralizing antibody against ZG16B. The shift in cell shape induced by ZG16B was reminiscent of a phenotype produced by TGFβ-treatment, consistent with epithelial-mesenchymal transition (EMT), and a change in cell–cell adhesion and motility.[19] Similarly, breast cancer cells produced a TGFβ-EMT-like response with the induction of fibronectin-1 and suppression of E-cadherin when exposed to ZG16B (Figure S5A,B). However, TGFβ did not stimulate ZG16B expression in T47D, MCF7 or MDA-MB-231 cells, suggesting the involvement of distinct mechanisms (Figure S5C).

In HME-hTert cells ZG16B weakened adhesion with fewer cells remaining attached after 5-min cycles of trypsinization and washing, was detected in a trypsin-sensitivity assay (Figure 2H). To determine whether ZG16B altered cell motility, a soluble factor was added to confluent monolayers after applying a uniform scratch. ZG16B greatly accelerated the closure of cell-free areas, which was inhibited by its neutralizing antibody (Figure 2I). In contrast, the combination of Bex and Carv effectively reduced cell migration (Figure 2J). These data indicated a marked impact of ZG16B on the phenotypic traits and the motility of non-malignant breast epithelial cells.

3.3 | Cellular functions inversely regulated by ZG16B and Bex + Carv

To elucidate the pharmacological potential of Bex + Carv to limit ZG16B-dependent pro-tumorigenic effects, their transcriptomic profiles were compared. RNA-seq analysis of HME-hTert cells identified 3240 genes as differentially expressed after Bex + Carv treatment and 1466 genes after ZG16B treatment, relative to controls. In total, 536 genes were regulated by both ZG16B and Bex + Carv (Figure 3A). Hierarchical clustering marked 158 genes as inversely regulated by ZG16B and Bex + Carv treatments. In addition, 118 genes that were suppressed by Bex + Carv and upregulated by ZG16B delineated three clusters. Categorized as biologically connected by

TABLE 1 Rank order of extracellular matrix and adhesion molecules upregulated by ZG16B in HME-hTert cells.

ZG16B-induced, extracellular matrix-related genes				
Gene symbol	**Differential expression**		**Gene name**	**Functional role in the ECM**
	Fold change	***p*-value**		
FN1	1.368	3.90E-31	Fibronectin 1	Connects integrins to ECM
PLEC	1.298	7.90E-39	Plectin	Interlinks cytoskeletal elements
COL5A1	1.297	6.31E-14	Collagen type V alpha 1 chain	regulates assembly of heterotypic collagen fibers
LAMA5	1.279	1.51E-18	Laminin subunit alpha 5	ECM glycoprotein of the BM
LAMA3	1.264	6.64E-15	Laminin subunit alpha 3	ECM glycoprotein of the BM
COL12A1	1.256	5.28E-10	Collagen type XII alpha 1 chain	Fibril-associated; modifies ECM interaction
HSPG2	1.254	2.77E-06	Heparan sulfate proteoglycan 2	Interacts with laminin, prolargin, collagen type IV
DYNC1H1	1.252	5.50E-14	Dynein cytoplasmic 1 heavy chain 1	Intracellular motility, microtubule-activated ATPase
COL4A2	1.250	3.43E-14	Collagen type IV alpha 2 chain	BM structural component
FBN1	1.247	7.09E-08	Fibrillin 1	Ca-binding ECM glycoprotein
TNC	1.239	9.97E-07	Tenascin C	Integrin ligand in the ECM
ITGB4	1.238	5.77E-26	Integrin subunit beta 4	Dimerization partner for int. α6 as laminin receptor
FBN2	1.233	1.12E-08	Fibrillin 2	Ca-binding ECM glycoprotein
PLXNA2	1.215	2.99E-08	Plexin A2	Cytoskeleton remodeling
FLNB	1.210	6.82E-13	Filamin B	Crosslinks cytoskeletal Actin filaments
VCAN	1.203	7.188E-04	Versican	ECM proteoglycan; cell adhesion, growth, migration
COL4A1	1.185	1.04E-05	Collagen type IV alpha 1 chain	BM structural component
TLN1	1.183	4.95E-10	Talin 1	Assembly of actin filaments; migration
LAMC1	1.181	3.46E-06	Laminin subunit gamma 1	ECM glycoprotein of the BM
LAMB3	1.180	8.41E-09	Laminin subunit beta 3	ECM glycoprotein of the BM
LAMB2	1.180	2.63E-05	Laminin subunit beta 2	ECM glycoprotein of the BM
VCL	1.176	4.44E-08	Vinculin	Membrane anchoring of F-actin
MYLK	1.172	1.231E-04	Myosin light chain kinase	Cytoskeletal contractile activity
LAMC2	1.170	8.34E-09	Laminin subunit gamma 2	ECM glycoprotein of the BM
MYH9	1.160	2.85E-09	Myosin heavy chain 9	Cytokinesis, cell shape and motility
AFAP1	1.159	1.133E-04	Actin filament associated protein 1	Adapter protein linking Src to Actin
FLNA	1.152	2.38E-10	Filamin A	Links Actin to membrane glycoproteins
COL7A1	1.151	1.031E-02	Collagen type VII alpha 1 chain	Anchoring epithelial cells to stroma
ITGA5	1.150	9.68E-06	Integrin subunit alpha 5	RGD receptor
ITGA2	1.144	1.395E-03	Integrin subunit alpha 2	Collagen receptor
LOXL2	1.143	1.377E-04	Lysyl oxidase like 2	Collagen, elastin crosslinker
ITGA3	1.141	2.26E-11	Integrin subunit alpha 3	Laminin receptor
COL4A6	1.139	2.046E-03	collagen type IV alpha 6 chain	BM structural component
ITGAV	1.137	1.684E-03	Integrin subunit alpha V	RGD receptor
LAMB1	1.133	3.540E-04	Laminin subunit beta 1	ECM glycoprotein of the BM
MACF1	1.132	1.423E-03	Microtubule Actin crosslinking factor 1	Couples microtubule to cellular junctions
FERMT1	1.118	2.583E-04	FERM domain containing kindlin 1	Regulates integrin activity
MMP15	1.115	4.665E-02	Matrix metallopeptidase 15	Remodeling, breakdown of ECM
ITGA6	1.113	6.03E-05	Integrin subunit alpha 6	Laminin receptor
ITGBL1	1.112	2.100E-02	Integrin subunit beta like 1	Dimerization partner for integrins α1-11

Abbreviations: BM, basal membrane; ECM, extracellular matrix.

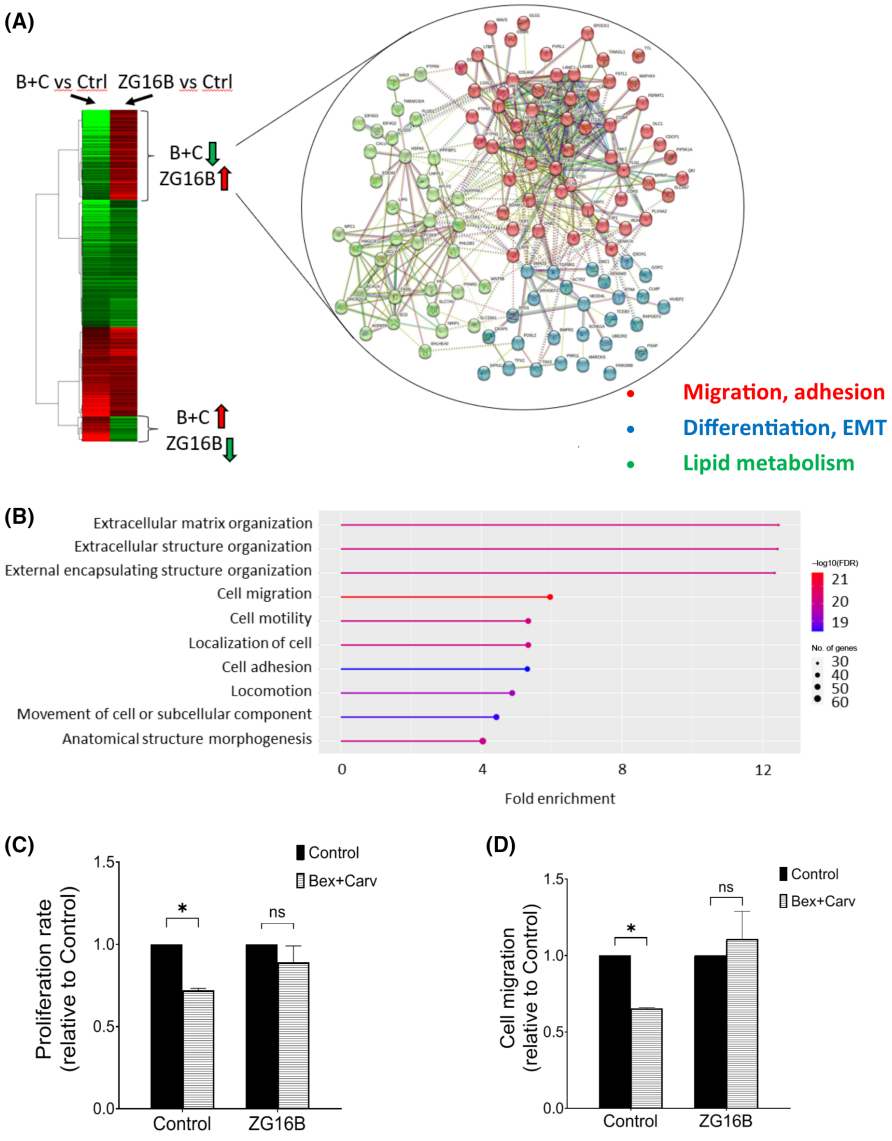

FIGURE 3 The intersection of cellular functions induced by ZG16B and suppressed by Bex + Carv. (A) Pathway and gene network analysis of genes downregulated by Bex + Carv and induced by ZG16B. (B) Gene ontology analysis of functional changes in response to ZG16B. (C) Changes in proliferation and (D) in motility of HME-hTert pre-treated with vehicle or Bex + Carv for 48 h, before adding control or ZG16B-enriched supernatants for 24 h.

String network analysis based on protein–protein interaction (PPI) enrichment score ($p < 1.0E-16$) these genes defined the cellular functions of ECM remodeling, cell adhesion, migration and lipid metabolism (Table S2).

Gene ontology analysis highlighted the functions of ECM organization and cell motility affected positively by ZG16B, but negatively by Bex + Carv (Figure 3B). In contrast, Bex + Carv-induced genes suppressed by ZG16B included several cytoskeletal genes associated with cell identity (Table S3).

To understand the relevance of ZG16B suppression in the cellular effects of Bex + Carv, next ZG16B was used in a 'rescue' experiment following a 48-h pre-treatment of HME-hTert cells by Bex + Carv. Repleting ZG16B by sequential administration restored both cell proliferation and motility to baseline levels (Figure 3C,D). Furthermore, Bex + Carv-induced basal characteristics, marked by elevated keratins 14 and 16, were abrogated by ZG16B (Figure S6). These results suggested that essential antitumor functions of the chemopreventive drug combination are tied to the suppression of ZG16B in normal cells.

3.4 | Breast cancer cells differentially respond to ZG16B in motility and growth

Scratch assays of ER-positive and triple-negative breast cancer cell lines demonstrated that ZG16B stimulated cell motility independently of their hormone receptor status (Figure 4A). Moreover, ZG16B-stimulated migration of MCF7 and MDA-MB-231 cells was blocked by PI3K inhibitor LY294002 (Figure 4B,C) and by the Akt inhibitor MK2206, indicating the involvement of the PI3K/Akt pathway in ZG16B activity. The inhibition of cell migration by LY294002 was associated with blocked Akt phosphorylation in response to ZG16B (lower panels, Figure 4B,C).

In contrast with motility, ZG16B had a differential impact on cell proliferation in ER-positive and ER-negative cell lines, as the growth of ER-negative MDA-MB-231, MDA-MB-468 or HCC1143 cells was impervious to ZG16B (Figure 4D). Concurrently, mitogenic signaling over Erk phosphorylation increased only in ER-positive T47D, but not in MDA-MB-231 cells, while Akt activation increased significantly in both (Figure 4E,F).

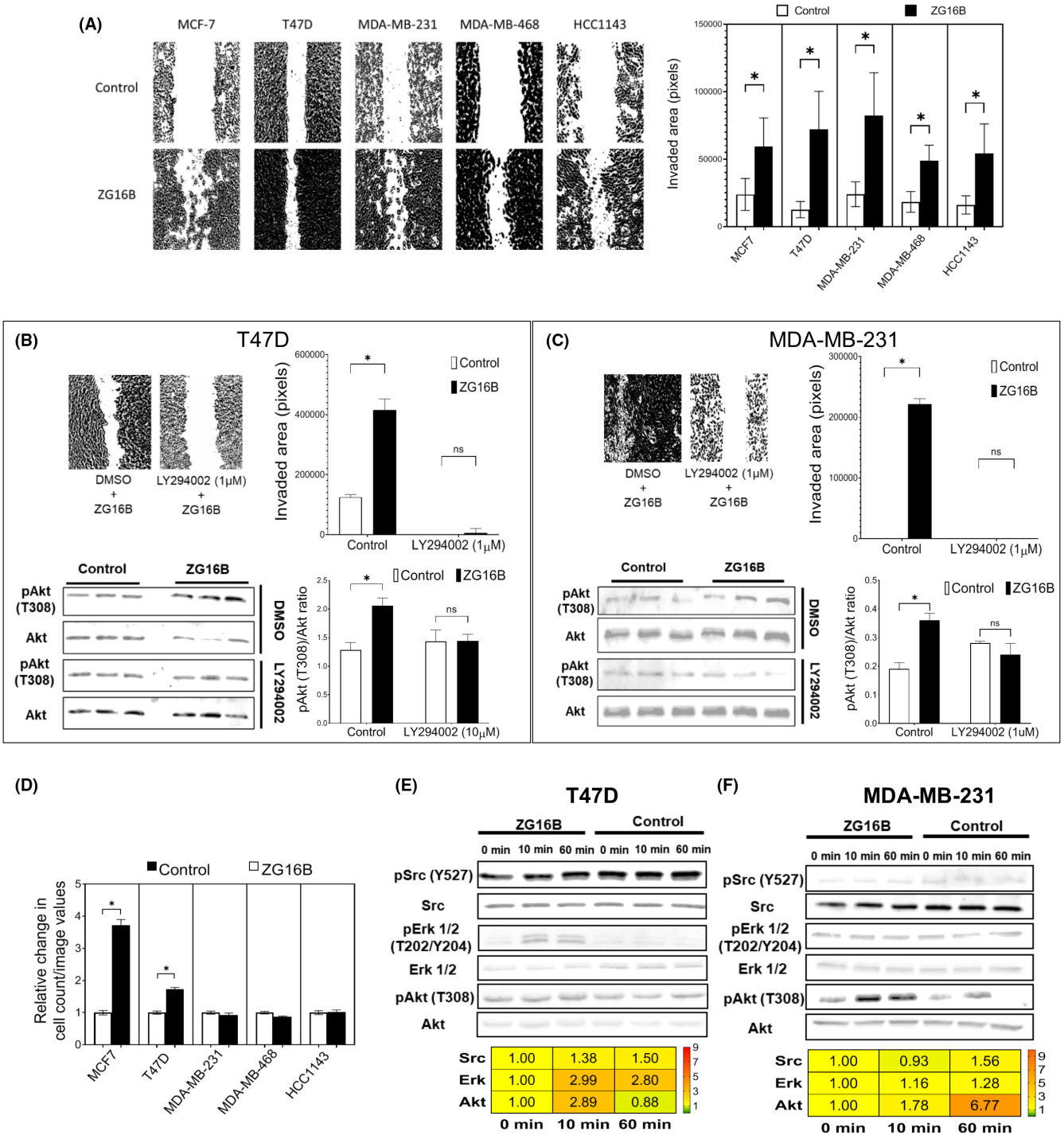

FIGURE 4 ER-independent, PI3K/Akt-mediated stimulation of cell motility by ZG16B in breast cancer cells. (A) Comparison of ZG16B-induced cell migration in ER-positive (MCF7, T47D) and ER-negative (MDA-MB-231, MDA-MB-468, HCC1143) breast cancer cell lines using scratch assays. (B) Cell motility and Akt phosphorylation were quantitated in T47D and (C) in MDA-MB-231 cells in the presence and absence of the PI3K inhibitor LY294002. ZG16B was applied for 24 h (scratch assay) or 10 min (western blot) to cells pre-treated with LY294002 (1 μM or 10 μM) for 1 h. (D) Comparison of proliferation rates in ER-positive and ER-negative breast cancer cell lines in response to ZG16B. (E) Comparison of the changes in phosphorylation levels of Src, Erk1/2 and Akt upon ZG16B treatment in T47D and (F) in MDA-MB-231 cells. Relative kinase phosphorylation levels normalized to total amounts are shown in heatmaps.

ZG16B enhanced clonogenic growth of MCF7, T47D, or MDA-MB-231 cells in soft agar (Figure 5A–C, left graphs). In contrast, colony formation was moderately inhibited by Bex or Carv, and more pronounced by the combination of Bex + Carv in all cell lines (Figure 5A–C, second graphs). Rexinoid-treated colonies contained decreased ZG16B mRNA levels, commensurate with the growth response (Figure 5A, right graph). Interestingly, while the expression of ZG16B in breast cancer cell lines was higher than in

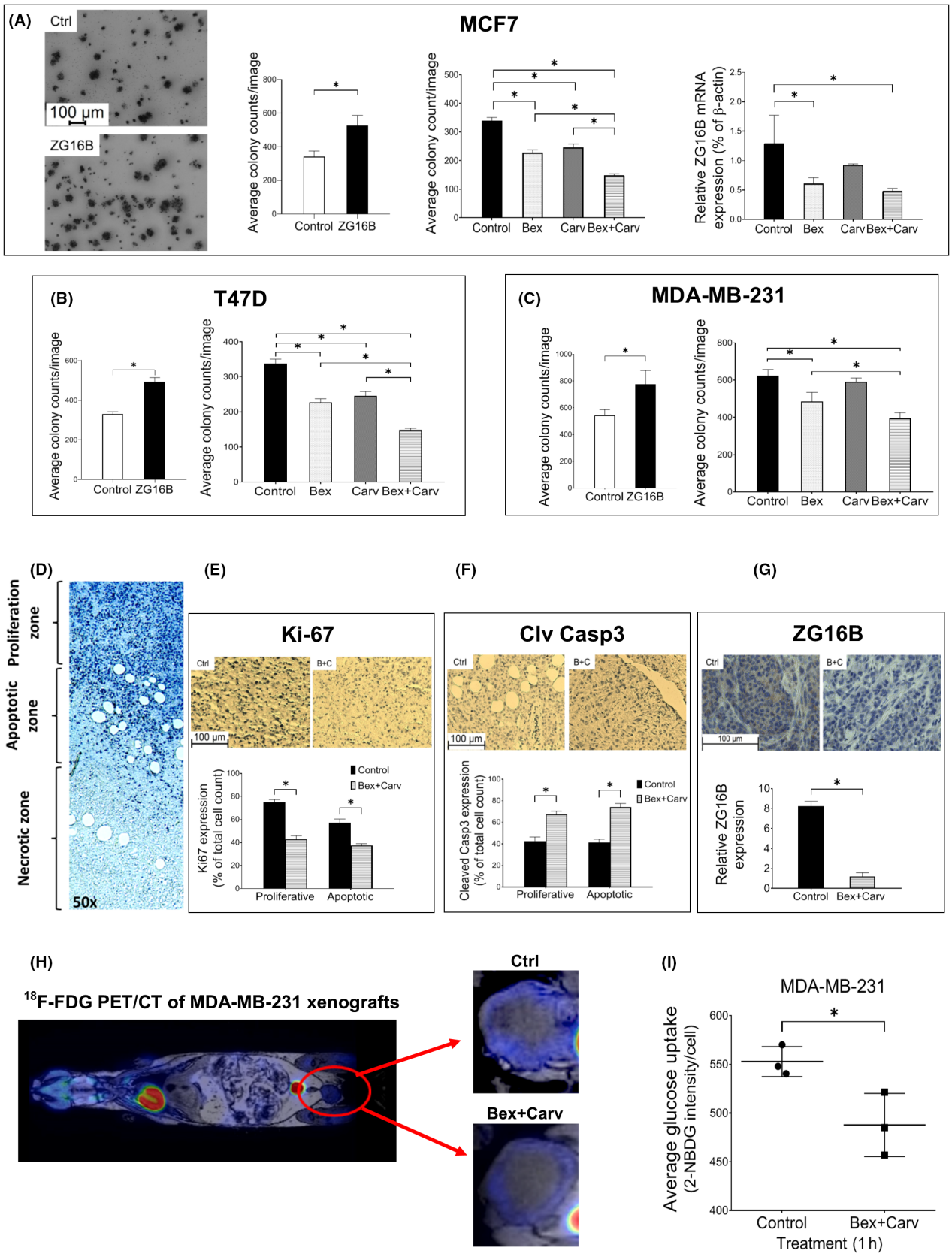

FIGURE 5 Bex + Carv suppresses ZG16B expression and growth of breast cancer cells in organoids and xenografts. (A) Anchorage-independent growth and ZG16B transcript levels in MCF7 tumor cell spheroids, in response to ZG16B-enriched supernatants, or Bex (1 μM) and Carv (1 μM). (B) Effects of ZG16B, Bex, Carv or Bex + Carv on colony formation in T47D and (C) MDA-MB-231 cells in soft agar assays. (D) Low-resolution microscopic cross-section of hematoxylin-stained xenograft of MDA-MB-231 cells. Changes in (E) Ki-67, (F) cleaved-Caspase3 (Clv-Casp3), and (G) ZG16B levels were detected by immunohistochemistry in xenograft sections. (H) Representative ^{18}F-FDG PET/CT image of SCID mice xenografted with MDA-MB-231 cells, treated by vehicle or Bex + Carv for 8 weeks. (I) Comparison of glucose uptake in MDA-MB-231 cells treated with vehicle or Bex + Carv.

normal cells, there was no general correlation with ARID1A levels (Figure S7).

To determine ZG16B expression in vivo, MDA-MB-231 cells were implanted and grown as xenografts in SCID mice. Tumor-bearing animals were treated with vehicle or Bex+Carv until tumor volumes reached 1000 mm^3. These triple-negative tumors formed an outer proliferative cell layer encapsulating a central necrotic and surrounding apoptotic zone (Figure 5D). ZG16B was expressed in the proliferative, but not the central or the apoptotic, zones of the lesions. In Bex+Carv-treated mice, immunostaining showed reduced Ki67 and abundant cleaved Caspase-3 levels in the proliferative and the apoptotic zones (Figure 5E,F). ZG16B expression was diminished in the xenografts from Bex+Carv-treated mice in the proliferating areas, relative to controls (Figure 5G). A comparison of the tumor gene expression profiles confirmed the upregulation of apoptosis-related genes, and suppression of ECM organization and cell-matrix interaction functions (Figure S8A,B).

Tumor growth and metabolic activity were monitored in parallel by positron emission tomography overlaid on NMR scans (PET-NMR, see Figure 5H). As the atypical activation of the PI3K/Akt pathway through ZG16B may promote glycolytic fluxes, we also assessed glucose uptake in response to Bex+Carv in the xenografts. PET-NMR images indicated a reduced ^{18}FDG uptake in Bex+Carv-treated tumors relative to controls, suggesting reduced metabolic activity. To rule out a systemic effect of Bex+Carv and assess their impact on tumor cell glucose metabolism, glucose uptake in cultured MDA-MB-231 cells was measured in response to Bex+Carv. The assay showed that a short-term, 1-h treatment was associated with a decrease in glucose uptake in vitro, confirming its potential to modulate metabolic activity (Figure 5I).

4 | DISCUSSION

Predicting the onset of carcinogenesis based on the initiating genetic alterations poses a challenge due to the large number of permutations that can potentially lead to malignancy. Conversely, prevention of cancer requires the suppression of enabling factors, such as proliferation, a favorable microenvironment or the creation of immune-privileged sites.[20] Rexinoids and carvedilol, clinical agents with known chemopreventive potential, have been shown to inhibit cell growth and carcinogenesis by various mechanisms.[16,21–23] We discovered that the combination of bexarotene and carvedilol consistently reduced ZG16B levels in non-malignant breast cells, soft agar-embedded organoids and orthotopic xenografts of breast tumor cells. It should be noted that, while in non-malignant breast cells the ARID1A-dependent recruitment of ZG16B amounts to a strong suppression of ZG16B and its pro-tumorigenic effects, this strategy would probably fail in ARID1A-deficient tumors.

ZG16B expression is elevated in breast cancer cells and tumor tissue, thus ZG16B was proposed as a prognostic marker in breast cancers.[9] Whether, and how ZG16B could contribute to carcinogenesis in breast cells remains elusive. The ability to alter cell–cell adhesion and relocate within tissue boundaries may act as enabling factors for carcinogenesis and invasion.[24] ZG16B overexpression was linked with the poor prognosis of various cancers due to enhanced cell migration and invasion.[5,6,25] Pancreatic tumorigenesis and resistance to therapy are associated with ECM formation around the tumor tissue, a process strongly promoted by ZG16B.[26] The relevance of ZG16B in linking matrix composition and tumor maintenance is emphasized by the development of anti-ZG16B-based therapy, currently tested in fast-tracked Phase 2 clinical trials of PBP1510 (NCT05141149) in patients with advanced pancreatic adenocarcinomas. As ZG16B was shown to regulate pancreatic cancer invasiveness, and targeted for the reduction of fibrotic tissue, understanding its role in the stromal context of the breast epithelium is critical. The dense stroma characterizing pancreatic ductal adenocarcinoma (PDAC) histology and the activation of EMT and TGFβ signaling represent similarities between basal-type pancreatic and mammary malignancies.[27] Stiffness of pancreatic cancers is known to increase invasive potential.[28] In the breast, increased mammographic density is a strong independent predictor for cancer formation and recurrence, with the highest breast cancer risk associated with the Her-2-positive subtype.[10,29] Studies demonstrated the role of compositional changes in matrisome proteins in breast cancer progression based on ECM proteins highly expressed in biopsies from invasive ductal carcinomas.[11,30] The association between altered characteristics of the tumor matrisome and cancer outcomes has also been shown.[12,31]

Our data clearly indicate that, beyond cellular adhesion and motility, ZG16B regulates determinants of stromal composition in breast cells and tissue. Specific ECM components associated with cell adhesion and ECM development in myoepithelial cells, including fibronectin-1, versican, laminins and fibulin2,[32] were induced by ZG16B and downregulated by Bex+Carv in HME-hTert cells. The upregulation of laminins, fibrillins, and collagen IV indicated a change toward matrix deposition and increased density.[33] Network forming components, such as fibronectin-1, collagen XII, talin, vinculin, and select integrins, may serve heightened mechanosensing and signal transduction.[14,34–37] Talin-1 and vinculin are key players to anchor F-actin to the focal adhesion assembly, form cell polarity, and also facilitate phosphatidylinositol-3 phosphate phosphorylation and activation of Akt.[38,39] Thus, mechanical forces transduced by mechanotransducers and select integrins in non-malignant cells play a major role in determining proliferative activity, stem cell-like phenotype and tumorigenic potential.[40–42]

ZG16B and Bex+Carv antagonize in defining cell identity, and suppressing or inducing basal characteristics, respectively. Induction of lamininα5 and β4-integrin by ZG16B may direct cells toward a luminal, along with a more estrogen-responsive state.[43] Furthermore, the downregulation of E-cadherin by ZG16B is commensurate with the loss of epithelial characteristics, decreased cell–cell adhesion and cancer progression.[44] Notably, the role of ZG16B differs in the context of carcinogenesis and cancer progression. The shift toward a mesenchymal phenotype is consistent with a metastasis-promoting activity of ZG16B in pancreatic cancers, where aberrant

stimulation from the microenvironment can inappropriately activate EMT, resulting in fibrosis or cancer progression, depending on the context.[45,46] In breast, the transformed mammary ECM may provide the mechanical signals that benefit the formation of tumor structure.[42] Increased fibronectin-1 levels, a shift in integrin isoforms upon ZG16B exposure and reduced epithelial cell adhesion allow tumor-promoting mesenchymal cells to migrate into the growing tumor mass.[47,48] Thus, our findings characterize ZG16B as a novel EMT inducer in breast cancer cells, supporting its potential role in metastatic breast cancers.

The inhibition of PI3K is a strategy pursued in the treatment of several cancers.[49] The impact of ZG16B on transformation-enabling factors appeared dependent on PI3K activity. Potential mechanisms of PI3K activation through ZG16B include the activation of CXCR4, α2/β1 integrin, collagen IVα2 and a stiff ECM network.[5,50–52] These insights provide further rationale for PI3K inhibitor-based combinations for breast cancer through the control of ECM regulation.[53]

In summary, we present a pharmacologic strategy repurposing the chemopreventive agents bexarotene and carvedilol as a novel combination to suppress ZG16B expression and its pro-tumorigenic functions. Restoration of ZG16B in Bex+Carv pre-treated cells restored their proliferative and migratory potential, demonstrating that the suppression of ZG16B by Bex+Carv is central to mediating inhibition of growth and motility in normal cells. The suppression of the pro-tumorigenic, ZG16B-promoted matrisome and motility, along with an anti-Warburg shift in glucose uptake in vivo may represent new hallmarks of the concerted tumor suppressive action by Bex+Carv.

AUTHOR CONTRIBUTIONS

Máté Lengyel: Data curation; formal analysis; investigation; methodology; visualization; writing – original draft. **Ádám Molnár:** Formal analysis; investigation. **Tamás Nagy:** Formal analysis; investigation. **Sham Jdeed:** Data curation; investigation. **Ildikó Garai:** Resources. **Zsolt Horváth:** Resources; validation; writing – review and editing. **Iván P. Uray:** Conceptualization; funding acquisition; investigation; project administration; resources; supervision; visualization; writing – review and editing.

ACKNOWLEDGMENTS

We thank Dr. Gergő Kalló and Dr. Éva Csősz at the UD Proteomics Core for their support with MS/MS peptide identification.

FUNDING INFORMATION

These studies were funded by grant K129218 from the National Research, Development and Innovation Office of Hungary (IPU). Support was provided by the European Social Fund GINOP 2.3.2–152,016–00020 MolMedEx program, the University of Debrecen Program for Scientific Publication, and the 37–11/2024 University of Debrecen Scientific Research Bridging Funds (DETKA, ÁOK to IPU). These studies were also supported by the ÚNKP-21-3 New National Excellence program of the Ministry for Innovation and Technology (ML).

CONFLICT OF INTEREST STATEMENT

The authors declare no conflict of interest.

ETHICS STATEMENT

Approval of the research protocol by an Institutional Review Board: All experiments were conducted in accordance with the guidelines approved by the University of Debrecen, the Hungarian Ethical Laws and regulations of the European Union.

Informed Consent: N/A.

Registry and the Registration No. of the study/trial: N/A.

Animal Studies: 16/2020/DEMÁB.

ORCID

Iván P. Uray https://orcid.org/0000-0002-3702-7608

REFERENCES

1. Cleator S, Heller W, Coombes RC. Triple-negative breast cancer: therapeutic options. *Lancet Oncol*. 2007;8(3):235-244.
2. Li Y, Zhang Y, Hill J, et al. The rexinoid, bexarotene, prevents the development of premalignant lesions in MMTV-erbB2 mice. *Br J Cancer*. 2008;98(8):1380-1388.
3. Liby K, Risingsong R, Royce DB, et al. Prevention and treatment of experimental estrogen receptor-negative mammary carcinogenesis by the synthetic triterpenoid CDDO-methyl ester and the rexinoid LG100268. *Clin Cancer Res*. 2008;14(14):4556-4563.
4. Jdeed S, Erdős E, Bálint BL, Uray IP. The role of ARID1A in the nonestrogenic modulation of IGF-1 signaling. *Mol Cancer Res*. 2022;20(7):1071-1082.
5. Lee Y, Kim SJ, Park HD, et al. PAUF functions in the metastasis of human pancreatic cancer cells and upregulates CXCR4 expression. *Oncogene*. 2010;29(1):56-67.
6. Youn SE, Jiang F, Won HY, et al. PAUF induces migration of human pancreatic cancer cells exclusively via the TLR4/MyD88/NF-kappaB signaling pathway. *Int J Mol Sci*. 2022;23(19):11414.
7. Yoo W, Choi H, Son YH, et al. Pancreatic cancer induces muscle wasting by promoting the release of pancreatic adenocarcinoma upregulated factor. *Exp Mol Med*. 2021;53(3):432-445.
8. Kim YJ, Jiang F, Park J, et al. PAUF as a target for treatment of high PAUF-expressing ovarian cancer. *Front Pharmacol*. 2022;13:890614.
9. Lu H, Shi C, Liu X, et al. Identification of ZG16B as a prognostic biomarker in breast cancer. *Open Med (Wars)*. 2021;16(1):1-13.
10. Duffy SW, Morrish OWE, Allgood PC, et al. Mammographic density and breast cancer risk in breast screening assessment cases and women with a family history of breast cancer. *Eur J Cancer*. 2018;88:48-56.
11. Tomko LA, Hill RC, Barrett A, et al. Targeted matrisome analysis identifies thrombospondin-2 and tenascin-C in aligned collagen stroma from invasive breast carcinoma. *Sci Rep*. 2018;8(1):12941.
12. Yuzhalin AE, Urbonas T, Silva MA, Muschel RJ, Gordon-Weeks AN. A core matrisome gene signature predicts cancer outcome. *Br J Cancer*. 2018;118(3):435-440.
13. Yui A, Oudin MJ. The rigidity connection: matrix stiffness and its impact on cancer progression. *Cancer Res*. 2024;84(7):958-960.
14. Kapoor A, Sen S. Synergistic modulation of cellular contractility by mixed extracellular matrices. *Int J Cell Biol*. 2012;2012:471591.
15. Shen Q, Uray IP, Li Y, et al. Targeting the activator protein 1 transcription factor for the prevention of estrogen receptor-negative mammary tumors. *Cancer Prev Res (Phila)*. 2008;1(1):45-55.
16. Uray IP, Dmitrovsky E, Brown PH. Retinoids and rexinoids in cancer prevention: from laboratory to clinic. *Semin Oncol*. 2016;43(1):49-64.

17. Jdeed S, Lengyel M, Uray IP. Redistribution of the SWI/SNF complex dictates coordinated transcriptional control over epithelial-mesenchymal transition of normal breast cells through TGF-beta; Signaling. *Cells*. 2022;11(17):2633.
18. Park HD, Lee Y, Oh YK, et al. Pancreatic adenocarcinoma upregulated factor promotes metastasis by regulating TLR/CXCR4 activation. *Oncogene*. 2011;30(2):201-211.
19. Kumar S, Das A, Sen S. Extracellular matrix density promotes EMT by weakening cell-cell adhesions. *Mol BioSyst*. 2014;10(4):838-850.
20. Dunn BK, Kramer BS. Cancer prevention: lessons learned and future directions. *Trends Cancer*. 2016;2(12):713-722.
21. Stanojkovic TP, Zizak Z, Mihailovic-Stanojevic N, Petrovic T, Juranic Z. Inhibition of proliferation on some neoplastic cell lines-act of carvedilol and captopril. *J Exp Clin Cancer Res*. 2005;24(3):387-395.
22. Sung CP, Arleth AJ, Eichman C, Truneh A, Ohlstein EH. Carvedilol, a multiple-action neurohumoral antagonist, inhibits mitogen-activated protein kinase and cell cycle progression in vascular smooth muscle cells. *J Pharmacol Exp Ther*. 1997;283(2):910-917.
23. Liang S, Shamim MA, Shahid A, et al. Prevention of skin carcinogenesis by the non-beta-blocking R-carvedilol enantiomer. *Cancer Prev Res (Phila)*. 2021;14(5):527-540.
24. Hui AY, Meens JA, Schick C, et al. Src and FAK mediate cell-matrix adhesion-dependent activation of met during transformation of breast epithelial cells. *J Cell Biochem*. 2009;107(6):1168-1181.
25. Barderas R, Mendes M, Torres S, et al. In-depth characterization of the secretome of colorectal cancer metastatic cells identifies key proteins in cell adhesion, migration, and invasion. *Mol Cell Proteomics*. 2013;12(6):1602-1620.
26. Kalli M, Poskus MD, Stylianopoulos T, Zervantonakis IK. Beyond matrix stiffness: targeting force-induced cancer drug resistance. *Trends Cancer*. 2023;9(11):937-954.
27. Cao L, Huang C, Cui Zhou D, et al. Proteogenomic characterization of pancreatic ductal adenocarcinoma. *Cell*. 2021;184(19):5031-5052 e26.
28. Nguyen AV, Nyberg KD, Scott MB, et al. Stiffness of pancreatic cancer cells is associated with increased invasive potential. *Integr Biol (Camb)*. 2016;8(12):1232-1245.
29. Bai S, Song D, Chen M, Lai X, Xu J, Dong F. The association between mammographic density and breast cancer molecular subtypes: a systematic review and meta-analysis. *Clin Radiol*. 2023;78(8):622-632.
30. Tasdemir N, Ding K, Savariau L, et al. Proteomic and transcriptomic profiling identifies mediators of anchorage-independent growth and roles of inhibitor of differentiation proteins in invasive lobular carcinoma. *Sci Rep*. 2020;10(1):11487.
31. Zhu J, Xiong G, Trinkle C, Xu R. Integrated extracellular matrix signaling in mammary gland development and breast cancer progression. *Histol Histopathol*. 2014;29(9):1083-1092.
32. Olijnyk D, Ibrahim AM, Ferrier RK, et al. Fibulin-2 is involved in early extracellular matrix development of the outgrowing mouse mammary epithelium. *Cell Mol Life Sci*. 2014;71(19):3811-3828.
33. Fiorino S, Di Saverio S, Leandri P, et al. The role of matricellular proteins and tissue stiffness in breast cancer: a systematic review. *Future Oncol*. 2018;14(16):1601-1627.
34. Kawano K, Kantak SS, Murai M, Yao CC, Kramer RH. Integrin alpha-3beta1 engagement disrupts intercellular adhesion. *Exp Cell Res*. 2001;262(2):180-196.
35. Shebanova O, Hammer DA. Biochemical and mechanical extracellular matrix properties dictate mammary epithelial cell motility and assembly. *Biotechnol J*. 2012;7(3):397-408.
36. Missirlis D, Heckmann L, Haraszti T, Spatz JP. Fibronectin anchoring to viscoelastic poly(dimethylsiloxane) elastomers controls fibroblast mechanosensing and directional motility. *Biomaterials*. 2022;287:121646.
37. Strohmeyer N, Bharadwaj M, Costell M, Fassler R, Muller DJ. Fibronectin-bound alpha5beta1 integrins sense load and signal to reinforce adhesion in less than a second. *Nat Mater*. 2017;16(12):1262-1270.
38. Atherton P, Stutchbury B, Wang DY, et al. Vinculin controls talin engagement with the actomyosin machinery. *Nat Commun*. 2015;6:10038.
39. Rubashkin MG, Cassereau L, Bainer R, et al. Force engages vinculin and promotes tumor progression by enhancing PI3K activation of phosphatidylinositol (3,4,5)-triphosphate. *Cancer Res*. 2014;74(17):4597-4611.
40. Mishra J, Chakraborty S, Niharika, et al. Mechanotransduction and epigenetic modulations of chromatin: role of mechanical signals in gene regulation. *J Cell Biochem*. 2024;125(3):e30531.
41. Uray IP, Uray K. Mechanotransduction at the plasma membrane-cytoskeleton Interface. *Int J Mol Sci*. 2021;22(21):11566.
42. Li C, Qiu S, Liu X, et al. Extracellular matrix-derived mechanical force governs breast cancer cell stemness and quiescence transition through integrin-DDR signaling. *Signal Transduct Target Ther*. 2023;8(1):247.
43. Englund JI, Bui H, Dinc DD, et al. Laminin matrix adhesion regulates basal mammary epithelial cell identity. *J Cell Sci*. 2022;135(23):jcs260232.
44. Bruner HC, Derksen PWB. Loss of E-cadherin-dependent cell–cell adhesion and the development and progression of cancer. *Cold Spring Harb Perspect Biol*. 2018;10(3):a029330.
45. Pastushenko I, Blanpain C. EMT transition states during tumor progression and metastasis. *Trends Cell Biol*. 2019;29(3):212-226.
46. Kalluri R, Neilson EG. Epithelial-mesenchymal transition and its implications for fibrosis. *J Clin Invest*. 2003;112(12):1776-1784.
47. Koorman T, Jansen KA, Khalil A, et al. Spatial collagen stiffening promotes collective breast cancer cell invasion by reinforcing extracellular matrix alignment. *Oncogene*. 2022;41(17):2458-2469.
48. Paramore SV, Goodwin K, Nelson CM. How to build an epithelial tree. *Phys Biol*. 2022;19(6):061002.
49. Davoodi-Moghaddam Z, Jafari-Raddani F, Delshad M, Pourbagheri-Sigaroodi A, Bashash D. Inhibitors of the PI3K/AKT/mTOR pathway in human malignancies; trend of current clinical trials. *J Cancer Res Clin Oncol*. 2023;149:15293-15310.
50. Long X, Wong CC, Tong L, et al. Peptostreptococcus anaerobius promotes colorectal carcinogenesis and modulates tumour immunity. *Nat Microbiol*. 2019;4(12):2319-2330.
51. Levental KR, Yu H, Kass L, et al. Matrix crosslinking forces tumor progression by enhancing integrin signaling. *Cell*. 2009;139(5):891-906.
52. De Martino D, Bravo-Cordero JJ. Collagens in cancer: structural regulators and guardians of cancer progression. *Cancer Res*. 2023;83(9):1386-1392.
53. Garcia AR, Mendes A, Custodia C, et al. Abrogating metastatic properties of triple-negative breast cancer cells by EGFR and PI3K dual inhibitors. *Cancers (Basel)*. 2023;15(15):3973.

SUPPORTING INFORMATION

Additional supporting information can be found online in the Supporting Information section at the end of this article.

How to cite this article: Lengyel M, Molnár Á, Nagy T, et al. Zymogen granule protein 16B (ZG16B) is a druggable epigenetic target to modulate the mammary extracellular matrix. *Cancer Sci*. 2024;00:1-14. doi:10.1111/cas.16382